RSC Advances

ROYAL SOCIETY OF CHEMISTRY

www.rsc.org/advances

RSC Advances

ARTICLE

Hydrogen Evolution on Nanostructured Ni-Cu Foams

D.S.P. Cardoso,[a] S. Eugénio,[b] T.M. Silva,[b,c] D.M.F. Santos,[a,*] C.A.C. Sequeira[a] and M.F. Montemor[b]

Received 00th January 20xx,
Accepted 00th January 20xx

DOI: 10.1039/x0xx00000x

www.rsc.org/

Three-dimensional (3D) nickel-copper (Ni-Cu) nanostructured foams were prepared by galvanostatic electrodeposition, on stainless steel substrates, using the dynamic hydrogen bubble template. These foams were tested as electrodes for the hydrogen evolution reaction (HER) in 8 M KOH solutions. Polarisation curves were obtained for the Ni-Cu foams and for a solid Ni electrode, in the 25-85 °C temperature range, and main kinetic parameters were determined. It was observed that the 3D foams have higher catalytic activity than pure Ni. HER activation energies for the Ni-Cu foams were lower (34-36 kJ mol^{-1}) than those calculated for t Ni electrode (62 kJ mol^{-1}). The foams also presented high stability for HER, which makes them potentially attractive cathode materials for application in industrial alkaline electrolysers.

Introduction

Hydrogen has received considerable attention as an energy carrier due to its large specific energy, high abundance in the universe, and "green" features, especially if produced using renewable energy sources.[1,2] However, due to the high costs involved in electrolytic water splitting, 96 % of hydrogen production is still obtained via hydrocarbon sources.[3,4] It is therefore important to focus in the reduction of the electrolysis cell voltage in order to minimise energy losses and improve the process efficiency. This can be achieved by decreasing the electrode overpotentials, by using electrodes with higher electrocatalytic activity.

The hydrogen evolution reaction (HER) is one of the most investigated reactions in electrochemistry. The electrodes used to enhance this reaction must possess a combination of specific characteristics, including high chemical stability, good catalytic activity (with low overpotential), high surface area, and low cost.[5] Nickel (Ni) is one of the most promising materials for this application, presenting more suitable properties when compared to other transition metals.[6] However, Ni electrodes tend to deactivate with time due to nickel hydrides formation.[7] Several routes have been developed to overcome this drawback, such as using Ni-based alloys with a spinel structure,[8] using amorphous or crystalline structure,[9-11] or even depositing metals onto Ni surfaces by magnetron sputtering.[12] Recently, the authors analysed Ni-rare earth (RE) alloys (with RE = Ce, Sm, Dy) that demonstrated increased electrocatalytic activity for HER compared to pure N electrode.[9,13] Copper (Cu) nanoparticles[14,15] and Ni-Cu composite electrodes[16,17] have also been reported as good electrocatalysts for HER.

Application of 3D macroporous materials for HER has already been reported to be advantageous.[18-20] Nanostructured metallic foams (NMFs) are 3D structures of interconnected pores with nano-ramified walls formed of metallic particles, dendrites or other morphologies that combine good electric and thermal conductivity with high surface area and low density. Such structures can be produced by electrodeposition in the hydrogen evolution regime where the evolving hydrogen bubbles act as a dynamic template to metal deposition.[21,22] By optimising the electrodeposition parameters it is possible to design nano-ramified foam structures with properly tailored architectures to enhance mass and charge transfer processes.

This work proposes the use of 3D Ni-Cu NMFs, formed by electrodeposition, as cathodes for the HER. The effect of the selected electrodeposition conditions is correlated with the foams morphology and, consequently, their activity for HER. Several parameters such as Tafel slopes, charge transfer coefficients, exchange current densities and activation energies were calculated to evaluate the HER performance in these electrodes.

Experimental

Preparation of the foam electrodes

Nickel-copper (Ni-Cu) nanostructured foams were electrodeposited on AISI 304 stainless steel substrates from an electrolyte solution containing 0.5 M $NiSO_4$, 1.5 M H_2SO_4, 1 M HCl and 0.01 M $CuSO_4$. This process was carried out in galvanostatic mode in a two electrode cell connected to a power source (Kikusui Electronic

[a] Center of Physics and Engineering of Advanced Materials (CeFEMA), Instituto Superior Técnico, Universidade de Lisboa, 1049-001 Lisboa, Portugal
[b] Centro de Química Estrutural (CQE), Instituto Superior Técnico, Universidade de Lisboa, 1049-001 Lisboa, Portugal
[c] Department of Mechanical Engineering, GI-MOSM, Instituto Superior de Engenharia de Lisboa, 1950-062 Lisboa, Portugal
* Corresponding author: diogosantos@tecnico.ulisboa.pt; Tel: +351 218417765

Model PAB 32-3) using a platinum plate as counter electrode. A cathodic current density of 2 and 3 A cm^{-2} was applied during 180 s for the electrodes preparation, named NiCu-2A and NiCu-3A, respectively. The geometric area of the foam electrodes was 1 cm^2.

Morphological and chemical characterisation

Surface morphology and chemical composition of the Ni-Cu metallic foams were analysed by scanning electron microscopy (SEM, Hitachi S2400) and energy dispersive X-ray spectroscopy (EDS, Rontec standard detector), respectively. SEM images and EDS spectra were acquired with an accelerating voltage of 25 kV. EDS analysis was performed at 3 different areas of the samples. A standardless EDS quantitative analysis was performed by Bruker Esprit software using the peak-to-background model (P/B) and subsequent ZAF correction.

Electrochemical measurements

Electrochemical measurements were performed using a PAR 273A potentiostat (Princeton Applied Research Inc.) controlled by PowerSuite software in a single-compartment glass cell of 125 mL volume. A three-electrode standard setup was used, where the Ni-Cu foam electrodes were used as working electrodes, while a Pt mesh (100 cm^2, Johnson Matthey) served as counter electrode, with saturated calomel electrode (SCE, HI 5412, Hanna Instruments) reference completing the circuit. All potentials in the paper were measured vs. SCE and then converted to the reversible hydrogen electrode (RHE) scale by using the formula $E_{RHE} = E_{SCE} + 1.115$ V (check electronic supplementary information for full details).

HER analysis was performed in 8 M KOH (Sigma-Aldrich, 90 wt.%) solutions. Millipore water was used for the solutions preparation. Linear scan voltammetry (LSV) measurements were used to scan the electrode potential from the open circuit potential (OCP, *ca.* -0.035 V) to -0.335 V vs. RHE, at a scan rate of 0.5 mV s^{-1}. A Ni planar electrode (A = 0.79 cm^2) was also tested for HER and its performance was directly compared to that of the two foam electrodes. Cell temperature was ranged between 25 and 85 °C, controlled by a water recirculation bath (Yellowline D-79219). Before each LSV measurement, a potential of -0.185 V vs. RHE was applied during 15 min to reduce any oxides existent on the electrodes surface. The stability of the electrodes was evaluated by running constant potential measurements (chronoamperometry). Current densities were calculated based on geometric area of the electrodes.

Results and discussion

Foams characterisation

The used electrodeposition parameters were based on previous experimental data[22] and chosen to obtain a fully developed 3D foam-like morphology. SEM analysis of the two Ni-Cu metallic foams (Fig. 1) revealed a uniform morphology, with a 3D structure presenting nearly-circular micrometric surface pores with non-compact walls formed of dendrites. Increase of applied current density, from 2 to 3 mA cm^{-2}, leads to a decrease of the surface pores density and to a broader distribution in pore size. NiCu-2A presents surface pores with an average area of 202 μm^2 and a density of 590 pores/mm^2. In the case of NiCu-3A the surface pore density is lower, 280 pores/mm^2, and the average pore area is 300 μm^2. If we consider that the surface pores are nearly circular, this corresponds to average pore diameters of 16 µm in NiCu-2A and 19 µm in NiCu-3A. These values are well in agreement with previous reports by the authors on the electrodeposition of Ni-Cu foams.[2] The different porosity exhibited by the two analysed foams can be attributed to the larger amount of metal deposited at higher currents, a result that is confirmed by the higher mass of NiCu-3A foam (Table 1). However, the dendritic structure of the pore walls is maintained (insets of Fig. 1) even when the higher current is applied.[2] It should also be noted that the values of pore density considered here are only relative to surface pores, i.e., pores visible at the surface of the foam. However, due to the interconnected porosity of the foams it is expected that the pore density in volume will have a much higher volume.

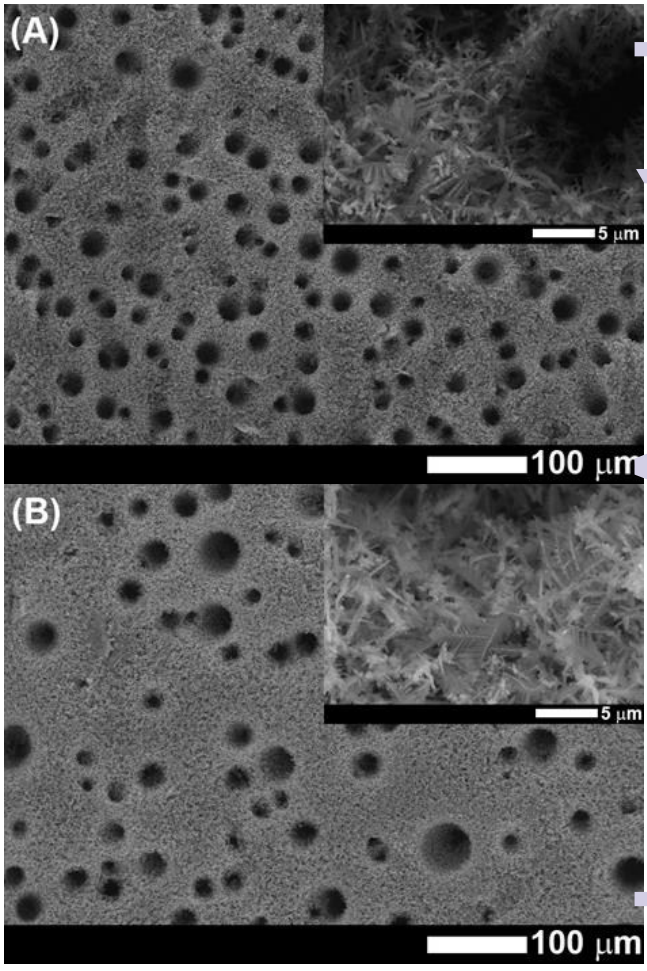

Fig. 1. SEM images of Ni-Cu metallic foams deposited on AISI 304 stainless steel for 180 s at (A) 2 A cm^{-2} and (B) 3 A cm^{-2}.

EDS analysis showed no significant differences between the chemical composition of NiCu-2A and NiCu-3A foams. Both materials have approximately 53 at.% of Ni and 47 at.% of Cu (Table 1).

Table 1. Electrodeposition conditions and chemical composition of Ni, NiCu-2A and NiCu-3A foam electrodes.

Sample	Electrodeposition conditions		Deposited mass / mg	Chemical composition / at.%	
	j / A cm^{-2}	t / s		Ni	Cu
NiCu-2A	2	180	34	52.9	47.1
NiCu-3A	3	180	41	52.7	47.3

Polarisation measurements

The activity of Ni-Cu foams and Ni planar electrodes for the HER was studied by LSV (ranging from OCP to -0.335 V) in the temperature range of 25-85 °C. The electrodes OCP tends to increase slightly with the temperature. Cathodic polarisation curves, *i.e.*, current density (j / mA cm^{-2}) as a function of the applied potential (E vs. RHE / V), for Ni, NiCu-2A and NiCu-3A, at 25 °C, are plotted in Fig. 2.

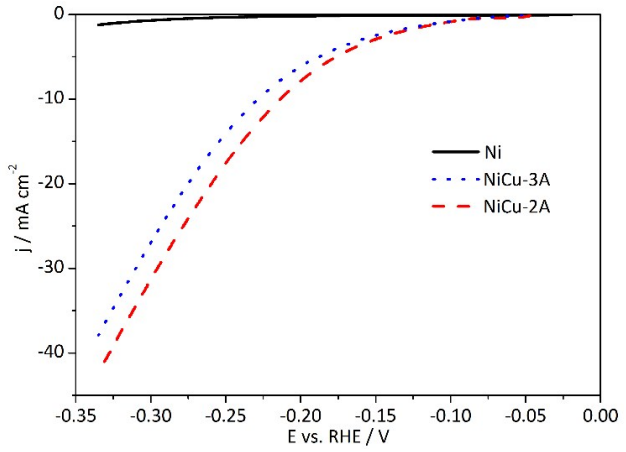

Fig. 2. Cathodic polarisation curves at 25 °C for Ni, NiCu-2A and NiCu-3A electrodes.

For a given potential value, the NiCu-2A and NiCu-3A foam electrodes are significantly more active than the Ni metal electrode, due to their higher surface area and chemical composition, as both factors strongly influence the electrodes performance for HER. The nanostructured morphology of the Ni-Cu foams (Fig. 1) leads to a higher ratio between real and geometric surface area, therefore contributing to an increase of the adsorbed hydrogen atoms at the electrode surface (Volmer step, eq. 1). Also, NiCu-2A leads to higher current densities than NiCu-3A. Taking into consideration that both electrodes have approximately the same chemical composition, this effect is attributed to the higher surface area of NiCu-2A, owing to a higher surface pore density (Fig. 1). On the other hand, the synergistic interaction of Ni and Cu can also contribute significantly to the HER efficiency.

It is well known that the increase of the electrocatalytic activity and intermetallic stability for HER is generally due to the bonding strengthening effect in the M-H_{ads} adsorbates. In alkaline media the HER mechanism is considered as a multi-step process (eqs. 1-3):[23]

$$H_2O + M + e^- \rightarrow MH_{ads} + OH^- \quad \text{(Volmer step)} \quad (1)$$

$$MH_{ads} + MH_{ads} \rightarrow H_2 + 2M \quad \text{(Tafel step)} \quad (2)$$

$$H_2O + MH_{ads} + e^- \rightarrow H_2 + M + OH^- \quad \text{(Heyrovsky step)} \quad (3)$$

The first discharge consists on the electrode surface coverage by adsorbed species (eq. 1). The following steps may involve a catalytic recombination of the adsorbed protons (MH_{ads}) via Tafel step (eq. 2), or an electrodesorption of the adsorbed intermediate via Heyrovsky step (eq. 3). Hence, and in agreement with Solmaz *et al.*[17], Ni-Cu foams enhanced electrocatalytic activity not only owes to their increased surface area (morphologic effect) but also to the synergistic interaction between Ni and Cu (electronic effect).

Accordingly, an intrinsic activity enhancement of the components has been reported,[16,17,24,25] with the resulting Ni-Cu alloy overpassing the electrocatalytic activity of the individual parent metals. In fact, Ni presents the highest exchange current density among the non-noble metals and is therefore considered a promising candidate for low-cost HER catalysts. However, the HER rate on Ni is hindered by the hydrogen desorption step, due to the large value of hydrogen binding energy on that metal. The combination of Ni with Cu, a low cost, high corrosion-resistant and environmental friendly material, leads to a decrease of the hydrogen binding energy and, consequently, to an enhanced HER activity of the Ni-Cu alloy when compared to Ni.

Based on the polarisation curves, the corresponding Tafel plots for the three electrodes, obtained for temperatures ranging from 25 to 85 °C, are shown in Fig. 3. When Ni-Cu foams are compared to the planar Ni electrode, the Tafel plots of the former show higher currents and lower η values, for the whole temperature range. This means that higher j values may be obtained at low η when using the produced foams, which could lead to lower electric energy consumption if using these Ni-Cu foams in a practical alkaline electrolyser.

Based on the Tafel plots (Fig. 3) and using the classic Tafel expression (eq. 4) it is possible to determine several parameters that characterise the HER on these electrodes. Tafel equation relates the overpotential, η, to the current density, j,

$$\eta = a + b \log j \quad (4)$$

where parameter a is the intercept associated to the exchange current density, j_0, which reflects the electron transfer intrinsic rate, and b is the Tafel slope, corresponding to the rate of change of the j with η.

Therefore, Tafel coefficients, b, were taken from the slope of the plots shown in Fig. 3, whereas charge transfer coefficients, α, and j_0 values were obtained using eqs. 5 and 6, respectively.

$$b = \frac{2.3RT}{\alpha F} \quad (5)$$

$$j_0 = 10^{-\frac{a}{b}} \quad (6)$$

where the ideal gas constant, R, is 8.314 J mol^{-1} K^{-1}, the temperature, T, is given in Kelvin, and Faraday's constant, F, is 96485 C mol^{-1}. The kinetic parameters calculated for the three tested electrodes are given in table 2. The modifications on the surface morphology clearly influence the reaction kinetics, and it should be emphasised that the Tafel slope on an electrode with an irregular surface will be necessarily different than that on an electrode with a flat surface.[26]

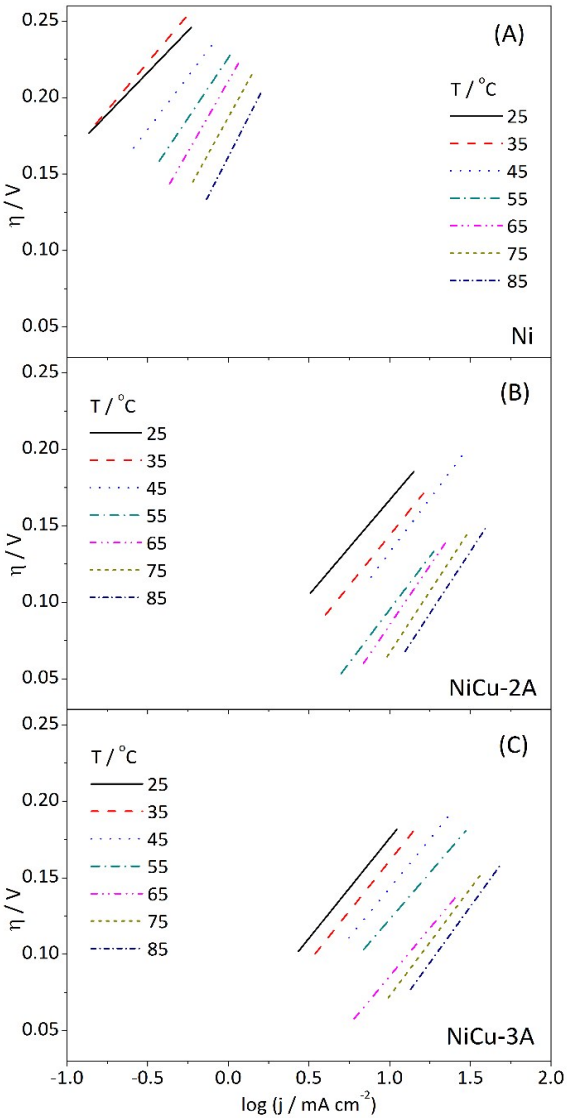

Fig. 3. Tafel plots for (A) Ni, (B) NiCu-2A and (C) NiCu-3A electrodes, for temperatures ranging from 25 to 85 °C.

As discussed before, the overall HER mechanism typically proceeds via two possible pathways, Volmer-Heyrovsky or Volmer-Tafel (eqs 1-3).[23] When the charge transfer coefficient, α, is 0.5 at 25 °C, the Tafel slope values being the rate determining step (RDS) the Volmer, Heyrovsky, and Tafel steps, are 120 mV dec^{-1}, 40 mV dec^{-1}, and 30 mV dec^{-1}, respectively. The obtained results suggest that the Volmer step is the RDS of the HER at the studied electrodes, followed by Heyrovsky step, with a negligible desorption reaction, as previously reported for other Ni-based electrodes.[9,13] Some effects such as the potential dependency of adsorbed intermediates at the surface, real surface area of the electrode and its roughness justify the differences between the theoretical and the experimental Tafel slopes.[27,28]

As shown in table 2, j_0 values obtained for HER at 25 °C with the Ni, NiCu-2A and NiCu-3A electrodes were 3.30 x 10^{-3}, 4.52 x 10^{-1} and 4.53 x 10^{-1} mA cm^{-2}, respectively. These values are higher than those reported for other Ni-based alloys.[25,29] Furthermore, Ni-Cu foams previously obtained by electrodeposition at currents low than those used in the present work (and which also contained a higher Ni content) led to j_0 values of one order of magnitude less. As pointed out by Krstajic *et al.*,[30] higher temperatures generally lead to higher j_0 values. Herein, increasing the temperature from 25 °C to 85 °C, increased the j_0 values (in mA cm^{-2}) in at least one order of magnitude: Ni (from 3.3 x 10^{-3} to 1.66 x 10^{-1}), NiCu-2A (from 4.52 x 10^{-1} to 4.74) and NiCu-3A (from 4.53 x 10^{-1} to 4.01).

HER was further evaluated by determining the activation energies, E_{act}. Arrhenius equation (eq. 7) was used for the calculation of E_{act} values, by plotting j_0 as a function of the reciprocal temperature (Fig. 4),

$$\ln j_0 = \ln A_i - \frac{E_{act}}{RT} \quad (7)$$

with A_i being the pre-exponential factor.

Based on the Arrhenius plots, obtained E_{act} values were 62, 36 and 34 kJ mol^{-1}, with R^2 values of 0.98, 0.99 and 0.98 for Ni, NiCu-2A and NiCu-3A electrodes, respectively. E_{act} values of the Ni-Cu foams are lower compared to those previously reported for Ni-RE electrodes studied in the same experimental conditions,[8,9] which range between 46 and 71 kJ mol^{-1}.

Table 2. Kinetic parameters for alkaline HER at Ni, NiCu-2A and NiCu-3A electrodes.

		T / °C						
		25	35	45	55	65	75	85
Ni	b / mV dec^{-1}	109	125	139	158	185	192	207
	α	0.54	0.49	0.45	0.41	0.36	0.36	0.34
	j_0 x 10^3 / mA cm^{-2}	3.3	5.2	16	37	72	106	166
NiCu-2A	b / mV dec^{-1}	124	131	140	139	155	161	162
	α	0.48	0.47	0.45	0.47	0.43	0.43	0.44
	j_0 x 10^3 / mA cm^{-2}	452	797	1135	2071	2825	3850	4740
NiCu-3A	b / mV dec^{-1}	131	132	129	132	126	140	146
	α	0.45	0.46	0.49	0.49	0.53	0.49	0.49
	j_0 x 10^3 / mA cm^{-2}	453	598	773	1245	2099	3033	4009

RSC Advances

ARTICLE

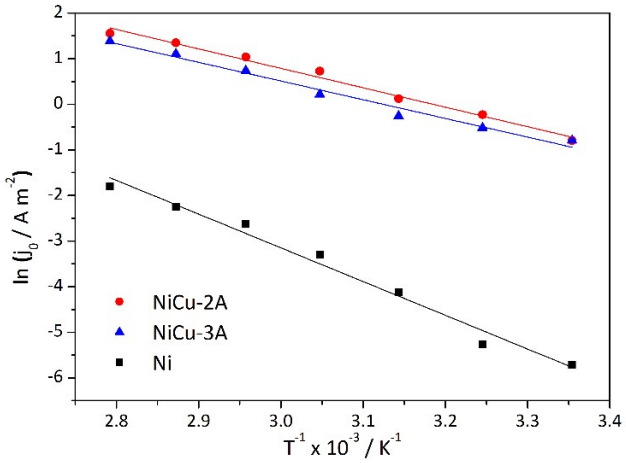

Fig. 4. Arrhenius plots for Ni, NiCu-2A and NiCu-3A electrodes.

The stability of the electrodes was evaluated by chronoamperometry (CA). Fig. 5 shows constant potential measurements at -0.185 and -0.285 V. In agreement with CV data, both NiCu-2A and NiCu-3A nanostructured foams presented higher currents than pure Ni. Furthermore, these currents were higher than those previously reported for Ni-Cu foams with higher Ni/Cu ratio.[18] The slow current decrease during CA measurements indicates a good stability of the electrodes. This was confirmed by the absence of alterations in electrolyte colour and electrode surface morphology after the experiments. However, considering the relatively short time of the experiments (60 minutes), the nature of stability cannot be fully characterised.

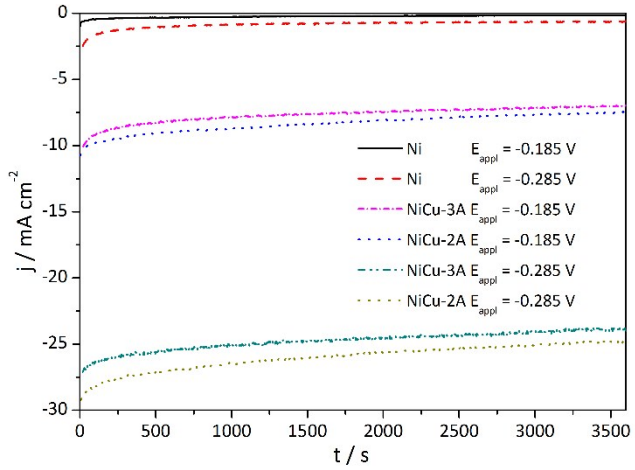

Fig. 5. CA curves of Ni and Ni-Cu electrodes at potentials of -0.185 V and -0.285 V, done at 25 °C.

Conclusions

3D nanostructured Ni-Cu metallic foams were prepared by galvanostatic electrodeposition and their performance for HER was evaluated. The foams led to significantly higher currents than a pure Ni electrode, which may be justified by an increase of the real surface area (as confirmed by SEM images) and by a synergistic interaction between the two alloy elements. Moreover, the Ni-Cu foam produced at lower current density exhibited the highest activity for HER, as justified by the larger pore density and consequently, higher area. Additionally, both Ni-Cu foams have shown high stability in the tested experimental conditions. Activation energies of 34–36 kJ mol^{-1} and 62 kJ mol^{-1} were obtained for Ni-Cu foams and for Ni electrode, respectively. In summary, these fast- and cheap-production foam electrodes were shown to have good catalytic activity and stability for HER, making them attractive cathode materials for industrial alkaline electrolysers.

Acknowledgements

D.M.F. Santos would like to thank Fundação para a Ciência e a Tecnologia (FCT, Portugal) for a contract within INVESTIGADOR FCT program (IF/01084/2014) as well as for funding a research grant within the project PTDC/SEN-ENR/121265/2010 (D.S.P. Cardoso). C. Eugénio and M.F. Montemor acknowledge FCT for financial support under the project PEst-OE/QUI/UI0100/2013 and COST actions MP1103-"Nanostructured materials for solid-state hydrogen storage" and MP1006-"Smart & green interfaces: From single bubbles/drops to industrial, environmental and Biomedical Applications".

Notes and references

1 A. Campen, K. Mondal and T. Wiltowski, *Int. J. Hydrogen Energy*, 2008, **33**, 332.
2 T.N. Veziroglu and F. Barbir, *Int. J. Hydrogen Energy*, 1992, **17**, 391.
3 M. Balat, *Int. J. Hydrogen Energy*, 2008, **33**, 4013.
4 M. Wang, Z. Wang and X. Gong, *Renew. Sustain. Energy Re*, 2014, **29**, 573.
5 B. Yazici, G. Tatli, H. Galip and M. Erbil, *Int. J. Hydrogen Energy*, 1995, **20**, 957.
6 H. Ezaki, M. Morinaga and S. Watanabe, *Electrochim. Acta*, 1993, **38**, 557.
7 R.M. Abouatallah, D.W. Kirk and J.W. Graydon, *Electrochim. Acta,* 2002, **47**, 2483.

8 M.E. Baydi, S.K. Tiwari, R.N. Singh, J-L. Rehspringer, P. Chartier, J.F. Koenig and G. Poillerat, *J. Solid State Chem*., 1995, **116**, 157.
9 D.M.F. Santos, L. Amaral, B. Sljukic, D. Macciò, A. Saccone and C.A.C. Sequeira, *J. Electrochem. Soc.*, 2014, **161**, F386.
10 T-C. Yuan, R-D. Li and K-C Zhou, *T. Nonferr. Metal. Soc*., 2007, **17**, 762.
11 M.V. Ananth and N.V. Parthasaradhy, *Int. J. Hydrogen Energy*, 1997, **22**, 747.
12 A.E. Mauer, D.W. Kirk and S.J. Thorpe, *Electrochim. Acta*, 2007, **52**, 3505.
13 D.S.P. Cardoso, L. Amaral, D.M.F. Santos, B. Šljukić, C.A.C. Sequeira, D. Macciò, and A. Saccone, *Int. J. Hydrogen Energy,* 2015, **40**, 4295.
14 B. Kumar, S. Saha, K. Ojha and A.K. Ganguli, *Mater. Res. Bull*., 2015, **64**, 283.
15 J. Ahmed, P. Trinh, A.M. Mugweru and A.K. Ganguli, *Solid State Sci*., 2011, **13**, 855.
16 Z. Yin and F. Chen, *J. Power Sources,* 2014, **265**, 273.
17 R. Solmaz, A. Döner, and G. Kardas, *Electrochem. Commun*., 2008, **10**, 1909.
18 D.M.F. Santos, S. Eugénio, C.A.C Sequeira and M.F. Montemor, *ECS Transactions*, 2015 (in press)
19 C.A. Marozzi and A.C. Chialvo, *Electrochim. Acta*, 2001, **46**, 861.
20 J. Zhang, M.D. Baró, E. Pellicer and J. Sort, *Nanoscale*, 2014, **6**, 12490.
21 H.C. Shin, J. Dong and M. Liu, *Adv. Mater*., 2003, **15**, 1610.
22 S. Eugénio, T.M. Silva, M.J. Carmezim, R.G. Duarte and M.F. Montemor, *J. Appl. Electrochem*., 2014, **44**, 455.
23 N. Krstajić, M Popović, B. Grgur and M. Vojnović, *J. Electroanal. Chem*., 2001, **512**, 16.
24 S.H. Ahn, H.-Y. Park, I. Choi, S.J. Yoo, S.J. Hwang, H.-J. Kim, E. Cho, C.W. Yoon, H. Park, H. Son, J.M. Hernandez, S.W. Nam, T.-H. Lim, S.-K. Kim and J.H. Jang, *Int. J. Hydrogen Energy*, 2013, **38**, 13493.
25 K. Ngamlerdpokin and N. Tantavichet, *Int. J. Hydrogen Energy*, 2014, **39**, 2505.
26 T. Pajkossy, *J. Electroanal. Chem*., 1991, **300**, 1.
27 M.F. Kibria, M.S.H. Mridha and A. H. Khan, *Int. J. Hydrogen Energy*, 1995, **20**, 435.
28 M.A. Domínguez-Crespo, A.M. Torres-Huerta, B. Brachetti-Sibaja and A. Flores-Vela, *Int. J. Hydrogen Energy*, 2011, **36**, 135.
29 F. Rosalbino, G. Borzone, E. Angelini and R. Raggio, *Electrochim. Acta*, 2003, **48**, 3939.
30 N. Krstajic, M. Popovic, B. Grgur, M. Vojnovic and D. Sepa, *J. Electroanal. Chem*. 2001, **512**, 27.